

Dynamic Phasor Modeling of Type 3 DFIG Wind Generators (Including SSCI Phenomenon) for Short-Circuit Calculations

Sriram Chandrasekar, *Member, IEEE*, and Ramakrishna Gokaraju, *Member, IEEE*

Abstract—Short-circuit modeling of wind generators is crucial to determine protective relay and control settings, equipment ratings, and to provide data for protection coordination. The short-circuit contribution of a Type 3 wind farm connected to a series-compensated line is affected by subsynchronous interactions, making it essential to model such behavior. Fundamental frequency models are unable to represent the majority of critical wind generator fault characteristics. The complete electromagnetic transient (EMT) models, though accurate, demand high levels of computation and modeling expertise. This paper proposes a novel modeling technique for a Type 3 wind farm based on the generalized averaging theory, where system variables are represented using time-varying Fourier coefficients known as dynamic phasors. The novelty and advantage of the proposed modeling technique is that it does not just include 60-Hz frequencies but also other dominant frequencies, such as 36 Hz, that are present due to the SSCI in the system. Methods currently used by the industry mostly rely on fundamental frequency-based analysis. Only the appropriate dynamic phasors are selected for the required fault behavior to be represented, improving computational efficiency. Once the SSCI behavior (waveforms showing resonant frequency at the point of common coupling) of a series-compensated Type 3 wind farm from real-time field data is available, the developed model could be used to simulate the scenario without necessarily having to know the exact control blocks of the wind generator controls. A 450-MW Type 3 wind farm, consisting of 150 units, was modeled using the proposed approach. The method is shown to be accurate for representing faults at the point of interconnection of the wind farm to the grid for balanced and unbalanced faults as well as for nonfundamental frequency components present in fault currents during subsynchronous interactions.

Index Terms—Dynamic phasors, generalized averaging, short-circuit modeling, type 3 wind generator.

I. INTRODUCTION

SEVERAL techniques have been proposed in the literature to model the short-circuit behavior of wind generators. Type 1 and Type 2 wind generators have been accurately modeled by simplified fundamental frequency representations. Reference [1] proposes wind turbine generator models for positive-sequence stability analysis. Reference [2] proposes

a modeling technique based on a voltage behind transient reactance (VBR) representation using sequence component networks to find the fault current at the inception of the fault.

Reference [3] proposes modeling using an expression for the short-circuit current and compares the results from tests on real induction machines, indicating that the model provides adequate representation. Reference [4] proposes a modeling approach where the short-circuit current is derived in the form of an analytical expression for an induction machine. The complexities affecting the short-circuit behavior of Type 1 and Type 2 wind generators are relatively fewer compared to the latest generation of wind generators. Reference [5] shows that for a Type 2 wind generator, the external rotor resistance value affects the damping of the short-circuit current with higher rotor resistance, contributing to further damping [6].

The short-circuit current of a Type 4 wind generator is regulated and limited to the rating of the power converter [7]. Hence, they can sufficiently be represented by a current source with an upper and lower limit based on the power converter rating for short-circuit analysis.

References [8]–[10] conclude that the aggregated model of the wind farm provides an accurate enough approximation of the performance of the wind farm for faults outside the wind farm.

It is relatively more complex to model the short-circuit behavior of the Type 3 wind generator compared to the other types of wind generators. LVRT requirements make it necessary for wind generators to stay connected to the grid and support the system for normally cleared disturbances [8], [11]. Hence, the unit protection for Type 3 generators is based on LVRT requirements. Reference [11] discusses the need for the LVRT feature and voltage profile maintenance in new wind turbine generator installations as well as retrofitting older generators. If the wind generator must stay connected to the grid, a facility has to be provided to bypass the high rotor current that occurs during faults and prevent damage to the rotor-side power-electronic circuits. This is done through crowbar circuits which are of two types, namely, active and passive crowbars, based on the power-electronic device used in the crowbar triggering circuit. The IEEE joint working group report [12] on fault current contributions from wind plants discusses the crowbar action but does not analyze in detail the difference between active and passive crowbar configurations.

Reference [13] shows that undamped subsynchronous oscillations, called subsynchronous control interactions (SSCI), could potentially occur in Type 3 wind turbine generators with

Manuscript received November 16, 2013; revised April 19, 2014 and July 07, 2014; accepted August 31, 2014. Date of publication October 29, 2014; date of current version March 20, 2015. Paper no. TPWRD-01291-2013.

The authors are with the University of Saskatchewan, Saskatoon, SK S7N 5A9 Canada (e-mail: src385@campus.usask.ca; rama.krishna@usask.ca).

Color versions of one or more of the figures in this paper are available online at <http://ieeexplore.ieee.org>.

Digital Object Identifier 10.1109/TPWRD.2014.2365587

power-electronic converters and controls that operate near series-compensated transmission lines. If left unmitigated, these oscillations can cause severe overvoltages, current distortion, and damage to the wind farm control circuits, such as in the case of the Texas event in 2009 [14].

A voltage-dependent current source model is proposed in [7] to represent Type 3 and Type 4 wind generator short-circuit behavior. The accuracy of this model depends on the level of accuracy of the model used to obtain the fault current envelopes.

The required capabilities for a modeling technique to be developed for a Type 3 wind farm are: 1) Capability to model balanced faults, unbalanced faults, and faults with subsynchronous interactions; 2) more sophisticated than fundamental frequency models, yet simpler than a detailed EMT model; and 3) capacity to selectively model only the required frequency components; and 4) the ability to simulate the SSCI interaction behavior from utility fault records without having to know the exact manufacturer controls.

The generalized averaging scheme which is also currently referred to by some authors as dynamic phasor modeling, was proposed by an MIT researcher in 1991 for modeling power converter circuits [15]. The essence of this scheme to model a periodically driven system, such as power converter circuits, is to retain only particular Fourier coefficients based on the interested system behavior under study, making it computationally efficient and inclusive of the required frequency components, even if nonfundamental in nature. Reference [16] discusses the application of generalized averaging model to large synchronous machines for symmetrical and unsymmetrical fault analysis. Reference [17] extends the application of this method to represent the dynamic behavior of a thyristor-controlled series capacitor (TCSC) in a simple yet accurate manner that is faster than detailed time-domain simulation. The generalized averaging model has been used to model synchronous machines and represent dynamic behavior of FACTS devices, such as the thyristor-controlled series capacitor (TCSC). References [18] and [19] utilize the generalized averaging scheme to model Type 1 and Type 3 wind generators, respectively, for short-circuit modeling. These models dealt with fundamental frequency-based modeling and were noninclusive of subsynchronous frequency control interactions.

The aforementioned works in the literature show that there has been a good amount of work on machine modeling of DFIG wind generators but not much research has been done on developing accurate models for fault analysis. The generalized averaging scheme using dynamic phasors is a very powerful concept for accurately modeling the Type 3 wind generator and its power electronics. This paper discusses the development of a dynamic phasor model for a Type 3 wind farm, including fundamental and nonfundamental subsynchronous frequencies, including fundamental and nonfundamental subsynchronous frequency effects.

Section II describes the short-circuit behavior of the Type 3 wind generator and briefly discusses the modeling complexities that affect its behavior. Section III describes the state-of-the-art short-circuit modeling schemes and their advantages and disadvantages. Section IV describes the dynamic phasor modeling method based on the generalized averaging theory (dynamic phasor modeling). Section V provides the results.

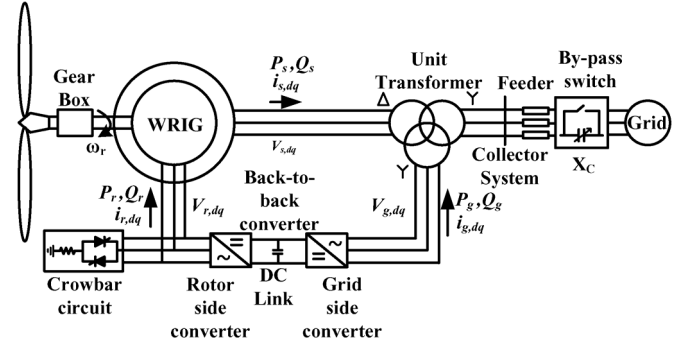


Fig. 1. Type 3 wind generator test system.

II. FAULT BEHAVIOR OF TYPE 3 WIND GENERATORS

A Type 3 wind turbine generator consists of a wound rotor induction generator where the rotor excitation is supplied by a back-to-back power converter. The rotor speed is allowed to vary within a slip range of $\pm 30\%$ [12].

The system shown in Fig. 1 consists of a 3-MW Type 3 wind generator connected to the collector system through a unit transformer and then to the grid through a feeder line. An equivalent model for a Type 3 wind farm consisting of multiple generators is explained in Section II-C. The transmission lines are series compensated in order to improve their power transfer capability, with the compensation providing a virtual reduction of the line reactance.

The various components of the test system are represented using differential equations expressed in the dq -reference frame rotating at synchronous speed ω_s . The test system is modeled based on the system parameters [13], which are given in Figs. 19, 20, and Table III. The generator is modeled using the classical 5th-order Park's equations [20]. The back-to-back converter is represented by a first-order model of a standard ac-dc-ac converter [21]. The rotor-side and grid-side converter controllers are defined by standard proportional-integral (PI) control-loop equations. The series-compensated transmission system and the transformer are modeled using lumped parameter models. The dynamic phasor form of these equations, which is the subject of this paper, are given in Section IV.

A. Crowbar Protection

The passive crowbar triggering circuit is constructed with thyristors which can be triggered into conduction using the gate signal and will remain conducting until the crowbar current is extinguished. The active crowbar triggering circuit is constructed with insulated-gate bipolar transistors (IGBTs), which can be turned off by reducing the gate-emitter voltage below a threshold value. Though different, both schemes use a resistor to bypass the excessive rotor current. Different measures may be used for the crowbar activation, such as rotor ac current or dc bus voltage, as well as different magnitude thresholds for each measure [12].

The value of the bypass resistor is of importance but not critical. It should be sufficiently low to avoid too large of a voltage on the converter terminals. On the other hand, it should be high enough to limit the current [22].

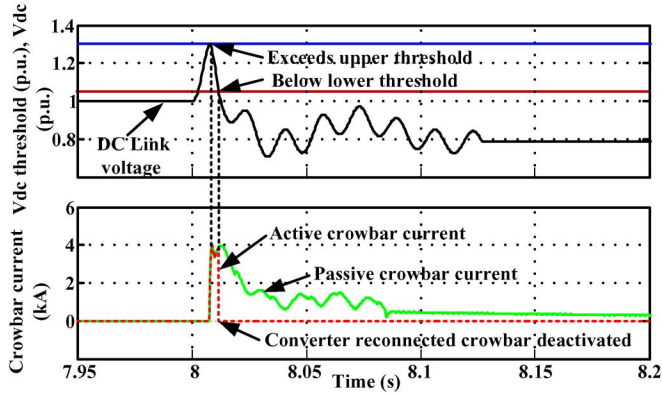


Fig. 2. Active and passive crowbar operation.

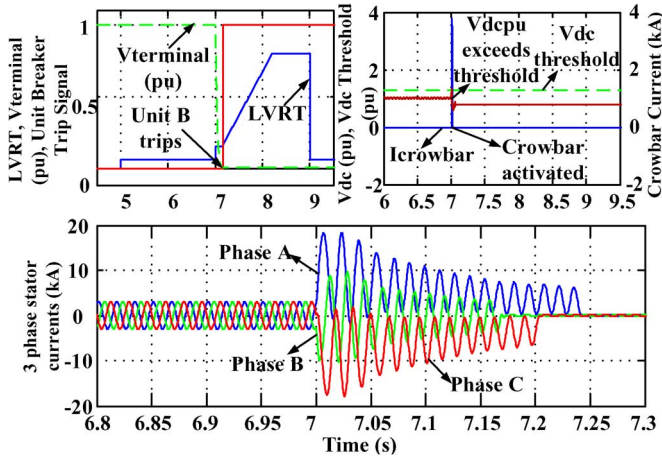


Fig. 3. Response of DFIG to a permanent three-phase fault.

Fig. 1 shows the passive crowbar configuration; however, the passive and active crowbar configurations were tested for a temporary three-phase fault at the terminals of the generator. Fig. 2 shows the difference between how these two schemes operate with respect to activating and deactivating the crowbar circuit during and after the fault occurrence.

Active crowbar control allows the Type 3 wind generator to have LVRT capability, that is, to reconnect the back-to-back converter as soon as possible after the fault occurrence. The LVRT characteristic utilized in the test system is shown in Fig. 3. The type of crowbar circuit and the LVRT-based protection strategies used affect the short-circuit behavior of the Type 3 wind generator and are important complexities that are considered for modeling.

Some DFIGs also utilize a chopper resistance on the dc-link capacitor instead of a rotor crowbar circuit. A study similar to the one mentioned in [23] shows that the DFIG fault current contribution was lower with a dc-link chopper when compared to that of a crowbar circuit.

B. Short-Circuit Behavior

The response of the generator to a permanent three-phase fault is shown in Fig. 3. In such a scenario, the crowbar is triggered and the unit breaker trips. When the dc-link voltage exceeds the upper threshold limit, a spike in the crowbar current indicating crowbar activation is shown. During the time interval

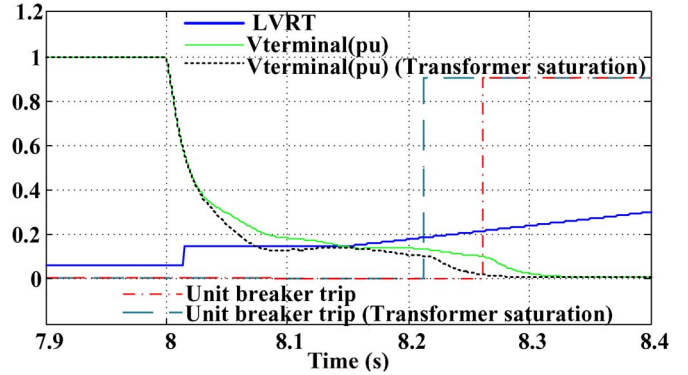


Fig. 4. Effect of transformer saturation on the terminal voltage during fault.

in which the crowbar resistance is connected to the rotor, the RSC is blocked and is not operating. Meanwhile, if the dc-link voltage goes below the lower threshold, then the crowbar is deactivated and the RSC is restarted and reconnected to the rotor. The tripping of the unit breaker is based on comparison of the terminal voltage and the LVRT curve. If and when the terminal voltage goes below the LVRT curve, the unit breaker trips. Fast Fourier transform (FFT) and Prony analysis of the phase A stator fault current reveals 60 Hz and the dc component to be the most dominant components.

Fig. 4 shows the effect of transformer saturation on the terminal voltage during the application of a three-phase permanent fault at the PCC. A comparison is shown between the terminal voltages with and without including the transformer saturation effects. Including the saturation effects leads to the unit breaker to trip earlier as the terminal voltage goes lower than the LVRT curve earlier.

C. Wind Farm Aggregation

The fault contribution from a wind farm can be accurately calculated without taking the collector impedances into account and the equivalencing of a wind farm can be made simple yet accurate by ignoring all cable impedances [6], [12].

An aggregate model of the Type 3 wind farm consisting of 150 wind generator units each rated at 3 MW is used to study its short-circuit behavior. This assumption is supported by several recent studies that suggest that wind farm aggregation provides a reasonable approximation for system interconnection studies [21]. A limitation of using an aggregate model is that this cannot be used to study faults internal to the wind farm, such as a fault at the terminals of one of the wind generator units.

D. Subsynchronous Control Interactions

SSCI phenomena for a Type 3 wind farm has been studied in [13] which also identifies the control loops in the RSC that are responsible for the subsynchronous interactions. This indicates how the SSCI phenomena can be attributed to the interaction between the series-compensated network and the power-electronic converter of the Type 3 wind generator. An EMT model was developed to be used as a benchmark model for the purpose of validating the dynamic phasor model. The SSCI phenomena was obtained by tuning the controller parameters (proportional gains of the PI controllers in the rotor current control

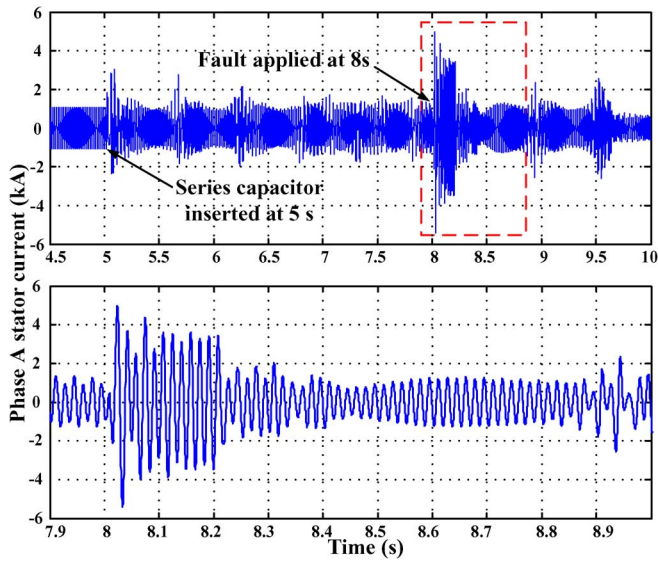


Fig. 5. Type 3 wind farm symmetrical fault current with SSCI frequency components and a magnified view immediately after the fault.

loops). These controller parameters were obtained using multiple time-domain simulations and a simplex optimization procedure to obtain the desired response behaviors. (No manufacturer control parameters were used.) In this kind of procedure, a detailed control design is not necessary and the optimum set of parameters could be obtained by simply repeating time-domain simulations. This kind of procedure has been used in the industry effectively in recent years for tuning control parameters for HVDC [24], FACTS, and generator controls.

The bypass switch of the series capacitor ($53.4 \mu\text{F}$), shown in Fig. 1, is opened 5 s after the start of simulation, thereby introducing a series compensation of 50% on the transmission line. Following this, a 200-ms three-phase fault is applied 8.0 s after the start of the simulation at the point of interconnection of the wind farm to the grid. The Phase A stator fault current measured is shown in Fig. 5. A buildup of subsynchronous oscillations can be observed.

Fig. 6 compares the phase A stator currents and rms voltage obtained from a straightforward three-phase fault and a three-phase fault with the SSCI component present. The magnitude of the fault current is significantly affected by the SSCI occurrence. This again confirms that models that are only able to represent the fundamental frequency components will be inaccurate for determining such complex fault behavior. The stator current waveform is scanned using FFT to determine the relative magnitude of the subsynchronous frequency component compared to the fundamental frequency component. Fig. 7 shows the relative magnitudes of the harmonic components of the phase A stator fault current waveform. The dominant frequency components are the 60-Hz and subharmonic frequency component ($\sim 36 \text{ Hz}$). These are shown as the first harmonic and 0.6 times the 1st harmonic, respectively.

An unsymmetrical fault (phase A to ground fault) also showed that SSCI has a significant impact on the magnitude of the fault current and that the fundamental frequency and the 36.5-Hz subsynchronous frequency components were dominant.

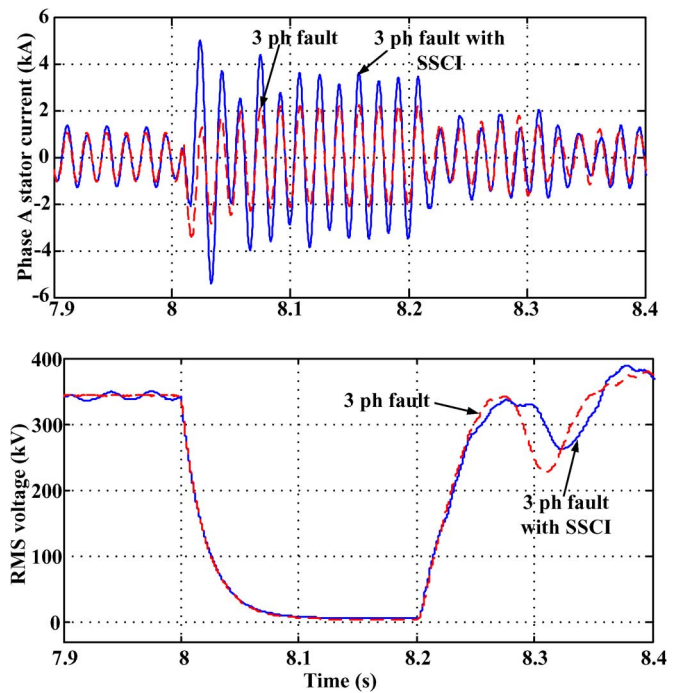


Fig. 6. Comparison of stator fault current and rms voltage without and with SSCI for a three-phase fault.

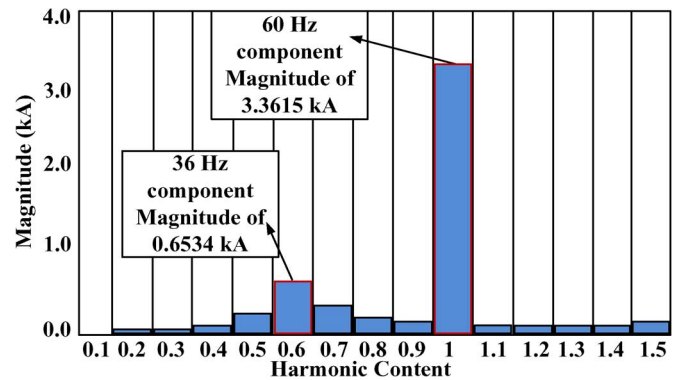


Fig. 7. FFT analysis of phase A symmetrical fault current with SSCI.

Fig. 8 shows the results of frequency scanning [25] for three different percentages of series capacitor compensation. This involves determining the magnitude and phase angle of the impedance when looking into the system from the generator terminals for all scanning frequencies [26]. For 50% compensation, there is a dip in the impedance magnitude and a corresponding change of sign of the phase angle at a frequency of 36.5 Hz. This frequency corresponds to the frequency of the subsynchronous component present in the stator current. Similar values for the other series capacitor compensation levels are also shown.

III. STATE-OF-THE-ART MODELING SCHEMES

This section briefly describes various modeling methods used in past literature to model wind generators versus a detailed EMT model. The inability of these models to represent the fault behavior of the Type 3 wind generator accurately is illustrated.

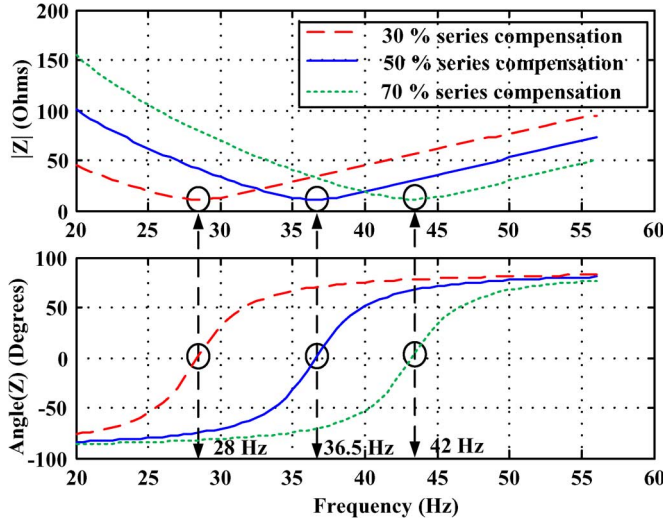


Fig. 8. Frequency scan: mag/phase plot of the network driving point impedance.

TABLE I
ACCURACY OF VBR MODELING FOR THE TYPE 3 WIND GENERATOR

Modeling	3 phase fault	Phase A-G fault
EMT	6.31 kA	4.80 kA
VBR	6.618 kA	3.8808 kA

Table I shows the accuracy of the voltage behind transient reactance (VBR) model [2] for representing the Type 3 wind generator's symmetrical and unsymmetrical fault behavior compared to the benchmark EMT model. It is not accurate for modeling Type 3 wind generators.

References [4] and [23] explain the analytical modeling method based on representing the short-circuit current behavior of wind generators by means of an analytical expression obtained for the stator fault current from the per-phase equations used to represent an induction machine for transient studies.

The expression for the phase A stator fault current is

$$I_{s_a} = \sqrt{2} \frac{V_s}{Z'} \left[e^{-t/T_s} \cos \alpha - (1-l) e^{j\omega_s t} e^{-t/T_r} \cos(\omega_s t + \alpha) \right]. \quad (1)$$

$L_{s\text{-eqv}}$ is the equivalent inductance looking from the stator into the short-circuited rotor given by $L_s + (L_r \parallel L_m)$, and $L_{r\text{-eqv}}$ is the equivalent inductance looking from the rotor into the short-circuited stator given by $L_r + (L_s \parallel L_m)$, where L_m is the mutual inductance. T_s and T_r are the damping time constants of the stator and rotor, respectively. They are computed using $T_s = L_{s\text{-eqv}}/R_s$ and $T_r = L_{r\text{-eqv}}/R_{r\text{-eff}}$. R_s is the stator winding resistance. $R_{r\text{-eff}}$ is the effective rotor resistance and varies with the wind generator type under study. L_s and L_r are the stator and rotor winding self inductances. l is the leakage factor, which is calculated as $1 - (L_m^2/L_s L_r)$. All rotor parameters refer to the stator side. Z' is the transient impedance and α is the voltage phase angle. The stator fault current for all wind generator types is obtained using (1); however, the calculation of T_r and Z' are dependent on the type of wind generator under study.

The accuracy of this mathematical model compared to the EMT model is shown in Fig. 9. This model is not as accurate

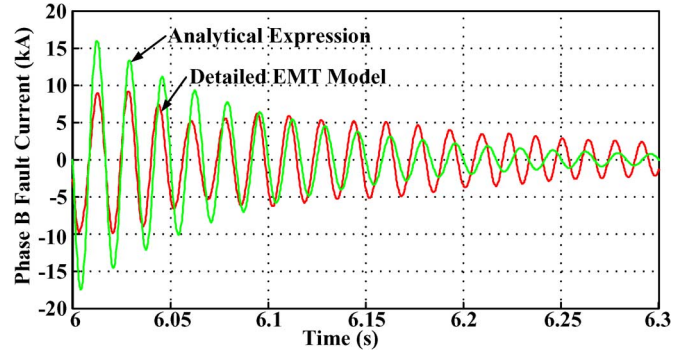


Fig. 9. Phase B stator currents—Type 3 wind generator—EMT model versus analytical expression.

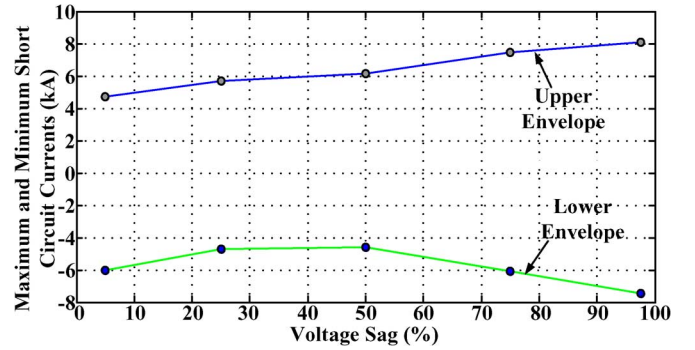


Fig. 10. Maximum and minimum short-circuit currents as a function of the percentage of voltage sag.

for Type 3 wind generators as for Type 1 and 2 wind generators. This model takes into account the effect of the crowbar resistance inclusion in the rotor circuit. However, since it considers the crowbar resistance to be included in the rotor circuit for the entire fault duration, this model would not be accurate for systems where manufacturers design the crowbar resistances to be activated and deactivated during the fault duration based on some signals, such as the dc-link voltage.

The voltage-dependent current-source (VDCS) modeling method is based on lookup tables as reported by a manufacturer [7]. These lookup tables contain data in the form of maximum and minimum short-circuit current values as a function of the point of interconnection voltage. The short-circuit data that form the lookup table can be obtained by measuring the maximum and minimum short-circuit current of the wind generator when the point of interconnection voltage is varied by applying voltage sags in the range of 20% to 90%. The maximum and minimum fault currents obtained for different percentage sags form the upper and lower fault current envelopes, respectively, as shown in Fig. 10.

The voltage-dependent current source model is capable of generating the short-circuit current characteristics of the Type 3 wind generator using a black-box-like approach. The accuracy of this model, that is, the accuracy of the short-circuit current envelopes, depends on the level of sophistication of the actual model used to obtain the maximum and minimum fault currents. In this case, a detailed EMT model was used for that purpose. It is clear that the voltage-dependent current source model is not a stand-alone model, since it requires the short-circuit current

values to be obtained from detailed EMT models or from the wind generator manufacturer.

IV. GENERALIZED AVERAGING OR DYNAMIC PHASOR MODELING

This proposed method of modeling can be used to only select the required frequency components to accurately represent the desired fault behavior of a Type 3 wind farm. The dynamic phasor modeling of DFIG has been reported in [27]. A real-valued periodic function having an angular frequency of $k\omega_s$ is represented by two components at k and $-k$. This model approximates the time-domain waveform $x(\tau)$ in the interval $\tau \in (t - T, t]$ by a Fourier series representation as

$$x(\tau) = \sum_{k=-\infty}^{\infty} \langle x \rangle_k(t) \cdot e^{jk\omega_s \tau} \quad (2)$$

where $\omega_s = 2\pi/T$ and $\langle x \rangle_k(t)$ is the k th time-varying Fourier coefficient, which is given by

$$\langle x \rangle_k(t) = \frac{1}{T} \int_{t-T}^t x(\tau) \cdot e^{-jk\omega_s \tau} d\tau. \quad (3)$$

The dynamic phasors are represented by $\langle x \rangle_k$ in the upcoming sections for the sake of simplicity. The appropriate dynamic phasors (Fourier coefficients) to accurately represent the short-circuit behavior of the Type 3 wind generator must be determined. The following properties of dynamic phasors are important in developing the model:

- 1) The derivative of the k th coefficient is given by

$$\frac{d\langle x \rangle_k(t)}{dt} = \left\langle \frac{dx}{dt} \right\rangle_k(t) - jk\omega_s \langle x \rangle_k(t). \quad (4)$$

- 2) The product of two time-domain variables is equal to a discrete time convolution of the two dynamic phasor sets of variables given by

$$\langle xy \rangle_k = \sum_{l=-\infty}^{\infty} \langle x \rangle_{k-l} \langle y \rangle_l. \quad (5)$$

The dynamic phasor model of the wind farm system is obtained from the dq equations of the individual components. Reference [28] shows an alternate approach of the dynamic phasor modeling ac machines using space vectors instead of dq equations.

By substituting the dq differential equations for different components of the test system described previously in (4), the dynamic phasor model equations are obtained. The selection of the set of dynamic phasors (also referred to as Fourier coefficients) for each of these components is based on the required short-circuit behavior to be studied, namely, a symmetrical or unsymmetrical fault with or without the influence of subsynchronous interactions. In a $dq0$ reference frame rotating at synchronous speed, the positive-sequence component will appear on the d and q axes as dc, that is, with frequency 0 ($k = 0$ for positive-sequence components), and the negative-sequence component will appear with a frequency of $2\omega_s$ ($k = 2$ for negative-sequence components). The zero-sequence component will appear on the 0 axis with a frequency of ω_s

TABLE II
SELECTION OF APPROPRIATE DYNAMIC PHASORS

Fault Condition	Dynamic phasors
Symmetrical Fault	$\langle x_{dq} \rangle_0$
Unsymmetrical Fault	$\langle x_{dq} \rangle_0, \langle x_{dq} \rangle_2$
Symmetrical Fault with SSCI	$\langle x_{dq} \rangle_0, \langle x_{dq} \rangle_{0.6}$
Unsymmetrical Fault with SSCI	$\langle x_{dq} \rangle_0, \langle x_{dq} \rangle_2, \langle x_{dq} \rangle_{0.6}$

($k = 1$ for zero-sequence components). The subsynchronous frequency dynamic phasor will be represented by $\langle x \rangle_{0.6}$ (36.5 Hz, which is approximately 0.6 times the system fundamental frequency of 60 Hz). Table II gives the dynamic phasors to represent different fault scenarios.

Substituting the dq equations of the different test system components into (4) and (5) yields the below dynamic phasor equations.

The turbine, shaft, and gear box are lumped together as a single equivalent mass. A multimass model would be required for studying phenomena, such as subsynchronous resonance. For studying subsynchronous control interactions, the equivalent mass model is sufficient. This is represented by

$$\frac{d\langle \omega_r \rangle_k}{dt} = \frac{\langle T_m \rangle_k - \langle T_e \rangle_k}{2H} - jk\omega_s \langle \omega_r \rangle_k \quad (6)$$

where electrical torque

$$\langle T_e \rangle_k = \langle \psi_{r,q} \cdot i_{r,d} \rangle_k - \langle \psi_{r,d} \cdot i_{r,q} \rangle_k. \quad (7)$$

The stator flux linkage due to the self-inductance of the stator circuit and the mutual inductance between the stator and rotor circuits is given by

$$\langle \psi_{s,dq} \rangle_k = L_{ss} \langle i_{s,dq} \rangle_k + L_{sr} \langle i_{r,dq} \rangle_k \quad (8)$$

and the corresponding stator voltage is

$$\langle V_{s,dq} \rangle_k = R_{ss} \langle i_{s,dq} \rangle_k + J\omega_s \langle \psi_{s,dq} \rangle_k + \frac{d\langle \psi_{s,dq} \rangle_k}{dt} - jk\omega_s \langle \psi_{s,dq} \rangle_k. \quad (9)$$

Similarly, the rotor flux linkage due to the self-inductance of the rotor circuit and the mutual inductance between the stator and rotor circuits is given by

$$\langle \psi_{r,dq} \rangle_k = L_{rr} \langle i_{r,dq} \rangle_k + L_{rs} \langle i_{s,dq} \rangle_k \quad (10)$$

and the corresponding rotor voltage is

$$\langle V_{r,dq} \rangle_k = R_{rr} \langle i_{r,dq} \rangle_k + J\langle \sigma \rangle_k \omega_s \langle \psi_{r,dq} \rangle_k + \frac{d\langle \psi_{r,dq} \rangle_k}{dt} - jk\omega_s \langle \psi_{r,dq} \rangle_k. \quad (11)$$

The slip, which is the normalized slip speed, is defined as

$$\langle \sigma \rangle_k = \frac{\omega_s - \langle \omega_r \rangle_k}{\omega_s} \quad (12)$$

where

$\psi_{r,d}$ and $\psi_{r,q}$	dq components of rotor flux linkage;
$\psi_{s,d}$ and $\psi_{s,q}$	dq components of stator flux linkage;
$i_{r,d}$ and $i_{r,q}$	dq components of rotor current;

$$\begin{aligned}
 i_{s,d} \text{ and } i_{s,q} & dq \text{ components of stator current;} \\
 i_{g,d} \text{ and } i_{g,q} & dq \text{ components of GSC-side current;} \\
 L_{ss} & \begin{bmatrix} L_s + L_m & 0 \\ 0 & L_s + L_m \end{bmatrix}; \\
 L_{rr} & \begin{bmatrix} L_r + L_m & 0 \\ 0 & L_r + L_m \end{bmatrix}; \\
 L_{sr} = L_{rs} & \begin{bmatrix} L_m & 0 \\ 0 & L_m \end{bmatrix}; \\
 V_{r,d} \text{ and } V_{r,q} & dq \text{ components of rotor voltage;} \\
 V_{s,d} \text{ and } V_{s,q} & dq \text{ components of stator voltage;} \\
 R_{ss} & \begin{bmatrix} R_s & 0 \\ 0 & R_s \end{bmatrix}; \\
 R_{rr} & \begin{bmatrix} R_r & 0 \\ 0 & R_r \end{bmatrix}; \\
 J & \begin{bmatrix} 0 & -1 \\ 1 & 0 \end{bmatrix}.
 \end{aligned}$$

In (11) for the rotor side, the crowbar resistance is modeled as a constant resistance. Whenever a fault is applied, the crowbar is activated only if the dc-link voltage exceeds the upper threshold value and is deactivated when it goes below the lower threshold. R_r is simply the rotor resistance when the crowbar is inactive and it includes the crowbar resistance when the crowbar is active. The back-to-back converter is represented by an average model as

$$C \frac{d\langle V_{dc} \rangle_k}{dt} = \langle m_{r,d} \cdot i_{r,d} \rangle_k + \langle m_{r,q} \cdot i_{r,q} \rangle_k - \langle m_{g,d} \cdot i_{g,d} \rangle_k - \langle m_{g,q} \cdot i_{g,q} \rangle_k - jk\langle V_{dc} \rangle_k. \quad (13)$$

The high-frequency switching dynamics of the back-to-back converter can be neglected since the phenomena under study is unaffected by these switching dynamics. The block diagrams for the rotor-side converter (RSC) and the grid-side converter (GSC) controllers are given in Figs. 19 and 20 and Table III [13]. The dynamics of these controllers are crucial for short-circuit analysis, especially in cases with potential subsynchronous control interactions.

The RSC provides an independent control of the stator-side active and reactive power by controlling the q -axis and d -axis rotor current. By tuning the RSC controller parameters (proportional gains of the PI controllers in the rotor current control loops), the SSCI phenomena was obtained [13]. The RSC controller is defined by the equations

$$\frac{d\langle x_{r,d} \rangle_k}{dt} = K_{I,P_s} (\langle P_s \rangle_k^* - \langle P_s \rangle_k) - jk\omega_s \langle x_{r,d} \rangle_k, \quad (14)$$

$$\langle m_{r,d} \rangle_k = \langle x_{r,d} \rangle_k + K_{P,P_s} (\langle P_s \rangle_k^* - \langle P_s \rangle_k), \quad (15)$$

$$\frac{d\langle x_{r,q} \rangle_k}{dt} = K_{I,Q_s} (\langle Q_s \rangle_k^* - \langle Q_s \rangle_k) - jk\omega_s \langle x_{r,q} \rangle_k, \quad (16)$$

$$\langle m_{r,q} \rangle_k = \langle x_{r,q} \rangle_k + K_{P,Q_s} (\langle Q_s \rangle_k^* - \langle Q_s \rangle_k). \quad (17)$$

The objective of the GSC is to keep the dc-link voltage at a constant value by controlling the q -axis grid-side current and regulating the reactive power exchange between the GSC and

the grid by controlling the d -axis grid-side current. The GSC controller is defined by the equations

$$\frac{d\langle x_{g,d} \rangle_k}{dt} = K_{I,V_{dc}} (\langle V_{dc}^* \rangle_k - \langle V_{dc} \rangle_k) - jk\omega_s \langle x_{g,d} \rangle_k, \quad (18)$$

$$\langle m_{g,d} \rangle_k = \langle x_{g,d} \rangle_k + K_{P,V_{dc}} (\langle V_{dc}^* \rangle_k - \langle V_{dc} \rangle_k), \quad (19)$$

$$\frac{d\langle x_{g,q} \rangle_k}{dt} = K_{I,i_{g,q}} (\langle i_{g,q}^* \rangle_k - \langle i_{g,q} \rangle_k) - jk\omega_s \langle x_{g,q} \rangle_k, \quad (20)$$

$$\langle m_{g,q} \rangle_k = \langle x_{g,q} \rangle_k + K_{P,i_{g,q}} (\langle i_{g,q}^* \rangle_k - \langle i_{g,q} \rangle_k). \quad (21)$$

The transmission system is modeled in order to include the effects of the series capacitor compensation since this is crucial to observe the SSCI phenomena. This ensures that not only fundamental frequency but also the nonfundamental frequency components are included. The series-compensated transmission system is modeled by the equations

$$L_{\text{line}} \frac{d\langle di_d \rangle_k}{dt} = \langle v_{s,d} \rangle_k - R_{\text{line}} \langle i_d \rangle_k + \omega_s L_{\text{line}} \langle i_q \rangle_k - \langle v_{c,d} \rangle_k - v_{b,d}, \quad (22)$$

$$L_{\text{line}} \frac{d\langle di_q \rangle_k}{dt} = \langle v_{s,q} \rangle_k - R_{\text{line}} \langle i_q \rangle_k - \omega_s L_{\text{line}} \langle i_d \rangle_k - \langle v_{c,q} \rangle_k - v_{b,q}, \quad (23)$$

$$C_{\text{line}} \frac{d\langle dv_{c,d} \rangle_k}{dt} = \langle i_d \rangle_k + \omega_s C_{\text{line}} \langle v_{c,q} \rangle_k, \quad (24)$$

$$C_{\text{line}} \frac{d\langle dv_{c,q} \rangle_k}{dt} = \langle i_q \rangle_k - \omega_s C_{\text{line}} \langle v_{c,d} \rangle_k. \quad (25)$$

The transformer is modeled using a constant impedance RL model as

$$L_t \frac{d\langle i_{t,d} \rangle_k}{dt} = \langle v_{pri,d} \rangle_k - \langle v_{sec,d} \rangle_k - R_t \langle i_{t,d} \rangle_k + \omega_s L_t \langle i_{t,q} \rangle_k - jk\omega_s L_t \langle i_{t,d} \rangle_k \quad (26)$$

$$L_t \frac{d\langle i_{t,q} \rangle_k}{dt} = \langle v_{pri,q} \rangle_k - \langle v_{sec,q} \rangle_k - R_t \langle i_{t,q} \rangle_k + \omega_s L_t \langle i_{t,d} \rangle_k - jk\omega_s L_t \langle i_{t,q} \rangle_k \quad (27)$$

where

m_d and m_q	modulation indices of the PWM converter;
V_{dc}	voltage across the dc-link capacitor (C);
P_g and P_r	real power flows at the GSC and RSC ends;
P_s^* and Q_s^*	reference values for the stator power;
P_s and Q_s	actual values for the stator power;
K_I and K_P	integral and proportional controllers gains;
V_{dc}	dc-link voltage;
$v_{s,d}$ and $v_{s,q}$	dq voltages at the high side of the substation;
$v_{c,d}$ and $v_{c,q}$	dq voltages across the capacitor;
$v_{b,d}$ and $v_{b,q}$	dq voltages of the grid/infinite bus;
R_t	resistance of the transformer winding;

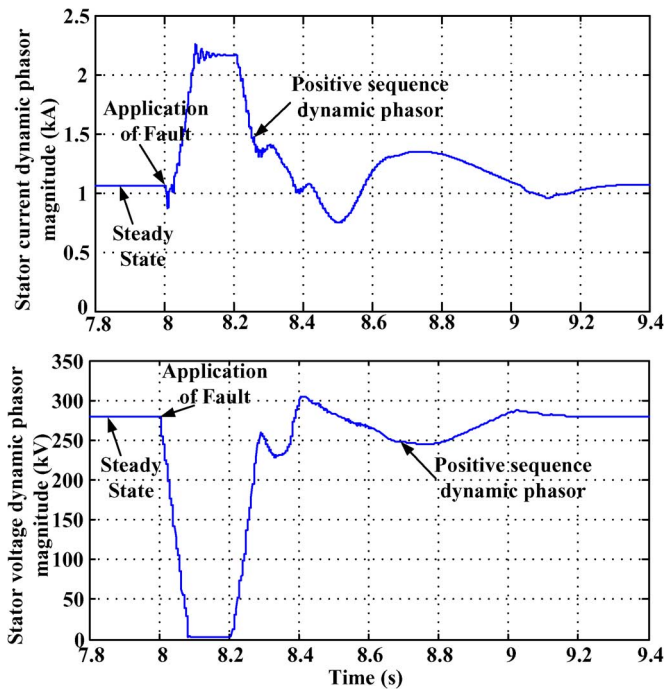


Fig. 11. Stator current and voltage positive-sequence dynamic phasor for three-phase symmetrical fault.

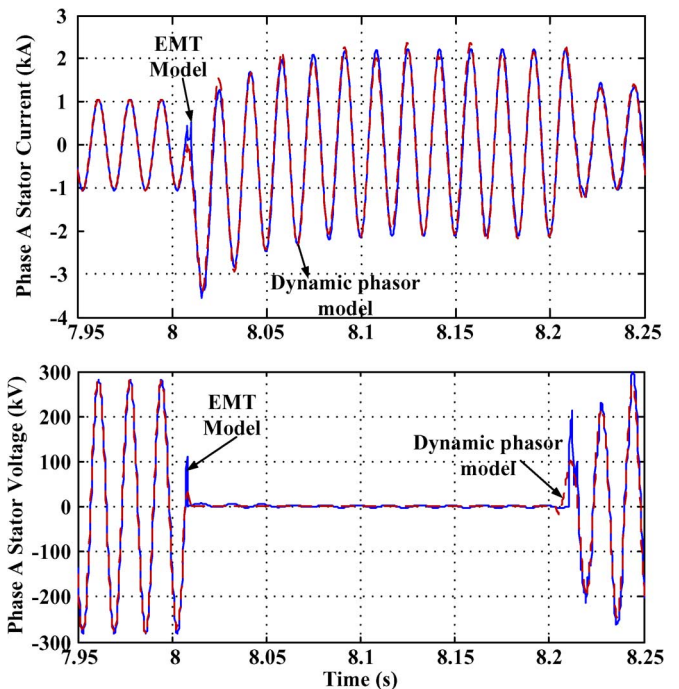


Fig. 12. Comparison of EMT and dynamic phasor modeling for the three-phase symmetrical fault.

L_t	inductance of the transformer winding;
$v_{pri,d}$ and $v_{pri,q}$	dq voltages of the transformer primary winding;
$v_{sec,d}$ and $v_{sec,q}$	dq voltages of the transformer secondary winding;
$i_{t,d}$ and $i_{t,q}$	dq currents of the transformer.

Solving these dynamic phasor dq equations gives the dynamic phasors/time-varying Fourier coefficients of all variables for every time step. Based on the type of fault and the percentage series compensation, as shown in Table II, only the relevant coefficients are chosen from the obtained values. For instance, the coefficients obtained for the stator current for different fault types are shown in Figs. 11, 13, 15, and 17.

V. SIMULATION RESULTS

A. Symmetrical Fault Behavior

The positive-sequence component of the current is the most dominant frequency component for the symmetrical fault condition. The appropriate choice of the required dynamic phasors (Fourier coefficients) to accurately represent the symmetrical short-circuit behavior would be the 60-Hz fundamental frequency coefficients (positive-sequence dynamic phasor). Negative-sequence dynamic phasors are not included since this is a symmetrical fault, and zero-sequence dynamic phasors are not included since the transformer is ungrounded. The selection of appropriate dynamic phasors was discussed previously in Table II. The positive-sequence dynamic phasor of the stator current and voltage for a 200-ms three-phase fault at the point of interconnection of the wind farm to the grid is shown in Fig. 11.

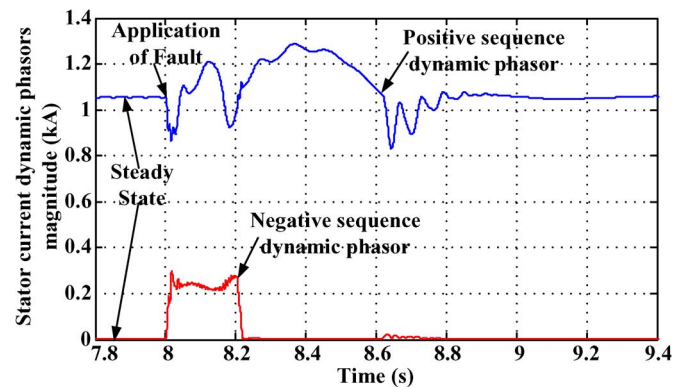


Fig. 13. Stator current positive- and negative-sequence dynamic phasors for a phase A-G fault.

The fault current and voltage output (phase A) for the symmetrical three-phase fault are shown in Fig. 12, which compares the EMT and dynamic phasor model results. The fault current waveforms show that the positive-sequence dynamic phasor is capable of accurately representing the symmetrical fault behavior of the Type 3 wind generator.

B. Unsymmetrical Fault Behavior

A 200-ms phase A to ground fault is applied at the point of interconnection of the wind farm to the grid. Both the positive- and negative-sequence dynamic phasors were chosen in order to accurately model the unsymmetrical fault behavior (zero-sequence dynamic phasors were not included since the transformer is ungrounded). Fig. 13 shows the positive- and negative-sequence dynamic phasors of the stator current.

The accuracy of the dynamic phasor model was assessed by comparison with the EMT model results. In order to represent

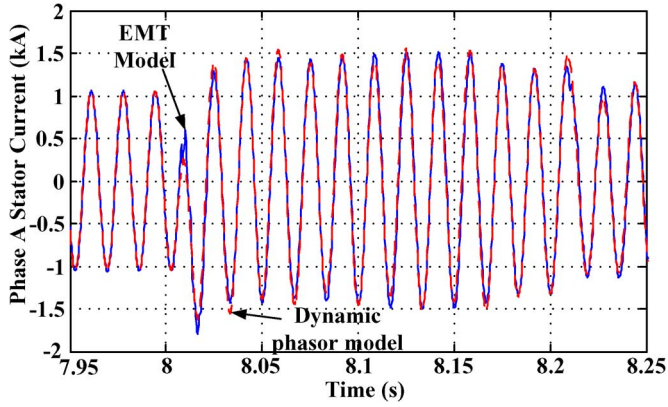


Fig. 14. Comparison of EMT and dynamic phasor modeling for Type 3 wind farm unsymmetrical fault application.

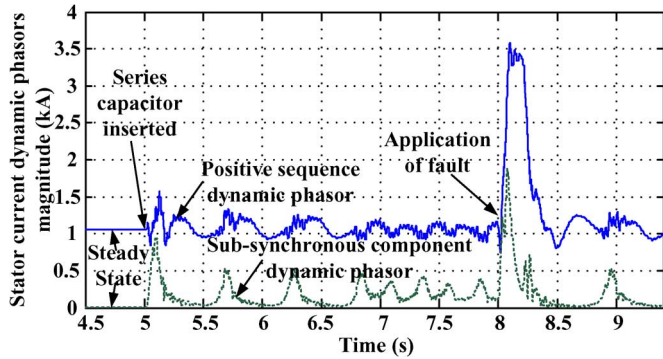


Fig. 15. Positive- and negative-sequence and subsynchronous component stator current dynamic phasors for a symmetrical fault in a series-compensated Type 3 wind farm.

the unsymmetrical fault behavior, the appropriate choice of Fourier coefficients would be the positive-sequence coefficient and the negative-sequence coefficient. Now, considering both of these components, the phase A stator fault current obtained from the dynamic phasor model is compared with the EMT simulation results as shown in Fig. 14. A high degree of accuracy was achieved with dynamic phasor representation.

C. Symmetrical Fault Behavior With SSCI

For accurate representation of this type of fault, as shown in Table II, the positive-sequence and subsynchronous component dynamic phasors are to be chosen. The negative-sequence dynamic phasor is not included since this is a symmetrical fault. Fig. 15 shows the relative magnitudes of the positive-sequence and subsynchronous component dynamic phasors of the stator current for a 200-ms three-phase fault applied at the point of interconnection of a series-compensated Type 3 wind farm to the grid.

Fig. 16 shows the comparison of the phase A fault current obtained from the EMT and the dynamic phasor modeling considering the fundamental and subsynchronous frequency Fourier coefficients. The accuracy of the dynamic phasor model is high, even for scenarios with subsynchronous oscillations.

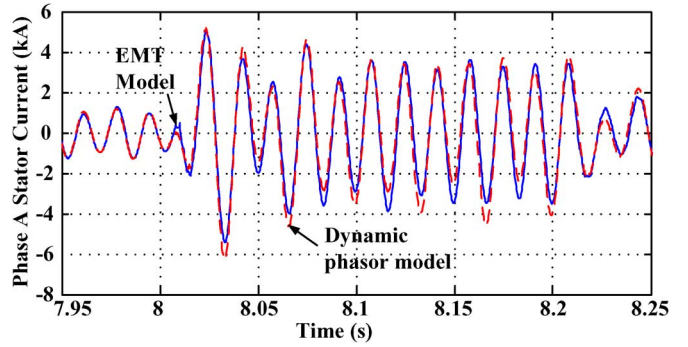


Fig. 16. Comparison of EMT and dynamic phasor modeling for the series-compensated Type 3 wind farm symmetrical fault application.

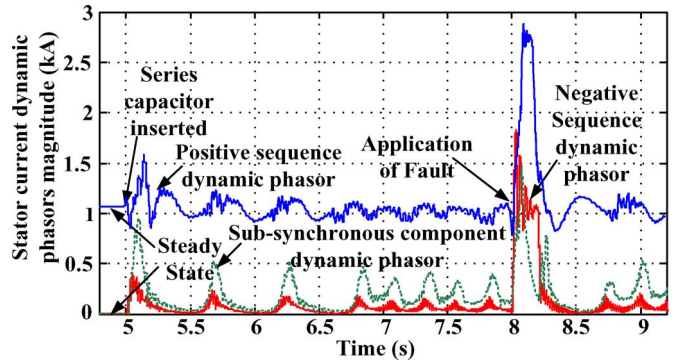


Fig. 17. Positive-sequence, negative-sequence, and subsynchronous component dynamic phasors for an unsymmetrical fault in a series-compensated Type 3 wind farm.

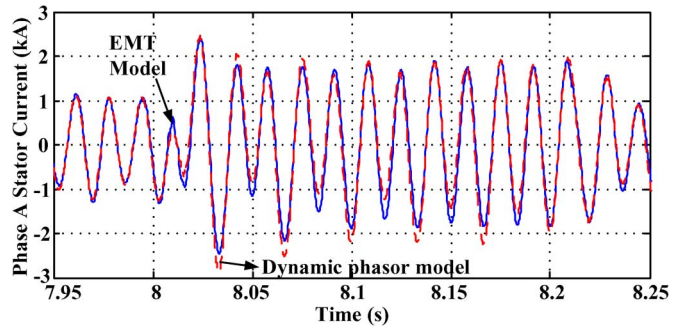


Fig. 18. Comparison of EMT and dynamic phasor modeling for the series-compensated Type 3 wind farm unsymmetrical fault application.

D. Unsymmetrical Fault Behavior With SSCI

The dynamic phasor model for the Type 3 wind farm is developed by choosing the appropriate Fourier coefficients, which are the positive-sequence, negative-sequence, and subsynchronous component dynamic phasors as explained in Table II. A 200-ms phase A to ground fault is applied at the point of interconnection of the wind farm to the grid. Fig. 17 shows the relative magnitudes of the dynamic phasors.

Using this selection of dynamic phasors, the model was developed and Fig. 18 shows the high accuracy achieved with the developed model compared to EMT results.

TABLE III
TYPE 3 WIND GENERATOR TEST SYSTEM DATA

Component	Parameters
Generator data	3.4 MVA , 0.69 kV , 60 Hz , $J = 1.856 \text{ s}$, $R_{stator} = 0.0054 \text{ p.u.}$, $R_{rotor} = 0.00607 \text{ p.u.}$, $L_m = 4.362 \text{ p.u.}$, $L_{stator} = 0.102 \text{ p.u.}$, $L_{rotor} = 0.11 \text{ p.u.}$
Crowbar circuit	$R_{crowbar} = 0.1 \Omega$, $R_{IGBT-ON} = 0.01 \Omega$, $R_{IGBT-OFF} = 1.0 \times 10^6 \Omega$, $V_{dc-UL} = 1.3 \text{ p.u.}$, $V_{dc-LL} = 1.05 \text{ p.u.}$
Back to back converter	$R_{IGBT-ON-GSC} = 0.0005 \Omega$, $R_{IGBT-ON-RSC} = 0.01 \Omega$, $R_{IGBT-OFF} = 1.0e6 \Omega$.
Rotor side controller	$K_{P,Q_s} = 1.0$, $K_{I,Q_s} = 1.0 \text{ s}$, $K_{P,P_s} = 1.0$, $K_{I,P_s} = 1.0 \text{ s}$, $K_{P,i_{r,d}} = 1.0$, $K_{I,i_{r,d}} = 2.0 \text{ s}$, $K_{P,i_{r,q}} = 1.0$, $K_{I,i_{r,q}} = 2.0 \text{ s}$
Grid side controller	$K_{P,Q_g} = 1.0$, $K_{I,Q_g} = 0.02 \text{ s}$, $K_{P,V_{dc}} = 1.0$, $K_{I,V_{dc}} = 0.02 \text{ s}$, $K_{P,i_{g,q}} = 0.1$, $K_{I,i_{g,q}} = 0.1 \text{ s}$, $K_{P,i_{g,d}} = 1.0$, $K_{I,i_{g,d}} = 0.02 \text{ s}$
Transmission line data	240 kms , $R_{Line} = 0.00003107 \text{ p.u./km}$, $X_{Line} = 0.0003479 \text{ p.u./km}$, $B_{Line} = 0.0051885 \text{ p.u./km}$
Transformer data	3.4 MVA , 60 Hz , $Y - Y - Y$, $0.482/33/0.688 \text{ kV}$, $X_{1-2} = 0.0888 \text{ p.u.}$, $X_{1-3} = 0.1663 \text{ p.u.}$, $X_{2-3} = 0.0875 \text{ p.u.}$

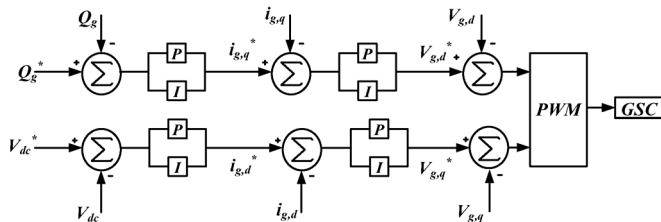


Fig. 19. Grid-side converter control block diagram.

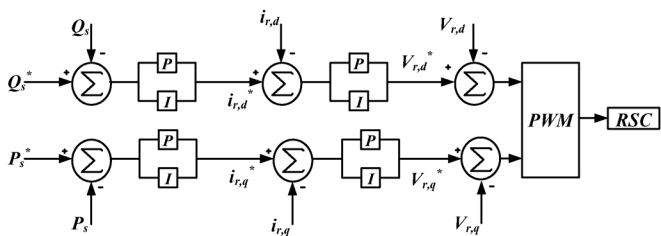


Fig. 20. Rotor-side converter control block diagram.

Using this modeling approach enables selective inclusion of only the appropriate dynamic phasors based on the fault behavior to be represented, making it computationally efficient. Unlike fundamental frequency approximations, this modeling method is capable of including nonfundamental subsynchronous frequency dynamic phasors for accurately representing SSCI effects. The methodology for the appropriate choice of these dynamic phasors was explained, and the proposed modeling technique was shown to be capable of accurately representing symmetrical and unsymmetrical faults with and without the occurrence of SSCI.

Since the dynamic phasor model of the Type 3 wind farm system is capable of accurately modeling not only fault current behavior, such as balanced and unbalanced faults, but also subsynchronous control interactions, it provides the necessary

information to design protection and control settings for wind farms. The model developed in this research will serve as a powerful tool for a utility engineer to design relay settings as well as control settings for damping SSCI oscillations for a Type 3 wind farm connected to a series-compensated transmission line.

VI. CONCLUSION

The Type 3 wind generator's short-circuit behavior is much more complex compared to other types of wind generators due to the relatively large number of factors that determine its behavior. This paper analyzed these factors and proposed a modeling technique to develop an accurate short-circuit model of a Type 3 wind farm. The advantage of this technique is that it is not based on fundamental frequency assumptions and, at the same time, is not as cumbersome to build as a detailed EMT model. It is based on the generalized averaging theory of representing power system variables using dynamic phasors or time-varying Fourier coefficients. This technique achieved a middle ground between conventional fundamental frequency-based electromechanical models and detailed EMT models with the ability to also represent nonfundamental frequencies accurately. This model can be used to selectively model only those frequency components required for the fault behavior under study. To simulate the SSCI, standard types of control blocks available in the literature were used. The model was shown to be capable of accurately representing symmetrical and unsymmetrical fault behavior as well as subsynchronous interactions compared with the benchmark EMT model.

REFERENCES

- [1] M. Asmine, J. Brochu, J. Fortmann, R. Gagnon, Y. Kazachkov, C. E. Langlois, C. Larose, E. Muljadi, J. MacDowell, P. Pourbeik, S. A. Seman, and K. Wiens, "Model validation for wind turbine generator models," *IEEE Trans. Power Syst.*, vol. 26, no. 3, pp. 1769–1782, Aug. 2011.
- [2] D. F. Howard, J. Restrepo, T. Smith, M. Starke, J. Dang, and R. G. Harley, "Calculation of fault current contribution of type 1 wind turbine generators," in *Proc. IEEE Power Energy Soc. Gen. Meeting*, Detroit, MI, USA, 2011, pp. 1–7.
- [3] S. S. Kalsi, B. Adkins, and D. D. Stephen, "Calculation of system fault currents due to induction motors," *Proc. Inst. Elect. Eng.*, vol. 118, no. 1, pp. 201–215, 1971.
- [4] J. Morren and S. W. H. de Haan, "Short circuit current of wind turbines with doubly fed induction generator," *IEEE Trans. Energy Convers.*, vol. 22, no. 1, pp. 174–180, Mar. 2007.
- [5] M. Chaudhary, S. M. Brahma, and S. J. Ranade, "Short circuit analysis of type II induction generator and wind farm," in *Proc. IEEE Power Energy Soc. Transm. Distrib. Conf. Expo.*, Montevideo, Uruguay, 2012, pp. 1–5.
- [6] S. Brahma, M. Chaudhary, and S. Ranade, "Some findings about equivalent windfarms with type 1 and type 2 induction generators," in *Proc. North Amer. Power Symp.*, Boston, MA, USA, 2011, pp. 1–6.
- [7] E. Gursoy and R. A. Walling, "Representation of variable speed wind turbine generators for short circuit analysis," in *Proc. IEEE Elect. Power Energy Conf.*, Winnipeg, MB, Canada, Oct. 2011, pp. 444–449.
- [8] C. Abbey, J. Morneau, J. Mahseredjian, and G. Joos, "Modeling requirements for transient stability studies for wind parks," presented at the IEEE Power Eng. Soc. Gen. Meeting, Montreal, QC, Canada, 2006.
- [9] M. Poller and S. Achilles, "Aggregated wind park models for analyzing power system dynamics," presented at the 4th Int. Workshop Large-Scale Integr. Wind Power Transm. Netw. Offshore Wind Farms, Billund, Denmark, Oct. 2003.
- [10] J. G. Sloopweg and W. L. Kling, "Aggregated modelling of wind parks in power system dynamics simulations," presented at the IEEE Power Tech Conf., Bologna, Italy, 2003.

- [11] I. Erlich and F. Shewarega, "Interaction of large wind power generation plants with the power system," in *Proc. IEEE Int. Power Energy Conf.*, Malaysia, 2006, pp. 12–18.
- [12] Joint Working Group on Fault Current Contributions from Wind Plants, "Fault current contributions from wind plants—Draft 7.1," IEEE Power Syst. Relaying Committee, San Diego, CA, USA, 2012, Tech. Rep..
- [13] G. D. Irwin, A. K. Jindal, and A. L. Isaacs, "Sub-synchronous control interactions between Type 3 wind turbines and series compensated AC transmission systems," presented at the IEEE Power Energy Soc. Gen. Meeting, Detroit, MI, USA, 2011.
- [14] North American Electric Reliability Corp., "Lesson learned—Sub-synchronous interaction between series-compensated transmission lines and generation," Atlanta, GA, USA, Rep. no. 20110705, Jul. 2011.
- [15] S. R. Sanders, J. M. Noworolski, X. Z. Liu, and G. C. Verghese, "Generalized averaging method for power conversion circuits," *IEEE Trans. Power Electron.*, vol. 6, no. 2, pp. 251–259, Apr. 1991.
- [16] A. M. Stankovic, B. C. Lesieutre, and T. Aydin, "Applications of generalized averaging to synchronous and induction machines," presented at the 28th North American Power Symp. M.I.T., Cambridge, MA, USA, Nov. 1996.
- [17] P. Mattavelli, G. C. Verghese, and A. Stankovic, "Phasor dynamics of thyristor-controlled series capacitor systems," *IEEE Trans. Power Syst.*, vol. 12, no. 3, pp. 1259–1267, Aug. 1997.
- [18] L. Piyasinghe, Z. Miao, and L. Fan, "Dynamic phase based model of type 1 wind generator for unbalanced operation," in *Proc. IEEE Power Electron. Mach. Wind Appl.*, Denver, CO, USA, 2012, pp. 1–5.
- [19] T. Demiray, F. Milano, and G. Andersson, "Dynamic phasor modeling of the doubly-fed induction generator under unbalanced conditions," in *Proc. IEEE Power Tech*, Lausanne, Switzerland, 2007, pp. 1049–1054.
- [20] P. Kundur, *Power System Stability and Control*. New York, USA: McGraw-Hill, 1994.
- [21] L. Fan, R. Kavasseri, Z. L. Miao, and C. Zhu, "Modeling of DFIG based wind farms for SSR analysis," *IEEE Trans. Power Del.*, vol. 25, no. 4, pp. 2073–2082, Oct. 2010.
- [22] J. Morren and S. de Haan, "Ridethrough of wind turbines with doubly-fed induction generator during a voltage dip," *IEEE Trans. Energy Convers.*, vol. 20, no. 2, pp. 435–441, Jun. 2005.
- [23] F. Sulla, "Fault behavior of wind turbines," Ph.D. dissertation, Dept. Meas. Technol. Ind. Elect. Eng., Lund Univ., Lund, Sweden, 2012.
- [24] S. Filizadeh, A. M. Gole, D. A. Woodford, and G. D. Irwin, "An optimization-enabled electromagnetic transient simulation-based methodology for hvdc controller design," *IEEE Trans. Power Del.*, vol. 22, no. 4, pp. 2559–2566, Oct. 2007.
- [25] B. Badrzadeh, M. Sahni, D. Muthumuni, Y. Zhou, and A. Gole, "Sub-synchronous interaction in wind power plants part I: Study tools and techniques," in *Proc. IEEE Power Energy Soc. Gen. Meeting*, San Diego, CA, USA, 2012, pp. 1–9.
- [26] D. H. R. Suriyaarachchi, U. D. Annakkage, C. Karawita, and D. A. Jacobson, "A procedure to study sub-synchronous interactions in wind integrated power systems," *IEEE Trans. Power Syst.*, vol. 28, no. 1, pp. 377–384, Feb. 2013.
- [27] D. Emmanuel and A. M. Stankovic, "Dynamic phasor modeling of the doubly-fed induction machine in generator operation," presented at the 4th Int. Workshop Large Scale Integr. Wind Power Transm. Netw. Off-shore Wind Farms, Denver, CO, USA, 2003.
- [28] A. M. Stankovic, S. R. Sanders, and T. Aydin, "Dynamic phasors in modeling and analysis of unbalanced polyphase ac machines," *IEEE Trans. Energy Convers.*, vol. 17, no. 1, pp. 107–113, Mar. 2002.



energy systems.



energy systems.

Sriram Chandrasekar (S'07–M'13) received the B.E. degree in electrical engineering from Anna University, Chennai, India, in 2007 and the M.Sc. degree in electrical engineering from the University of Saskatchewan, Saskatoon, SK, Canada, in 2013.

During 2007–2010, he was a Software Engineer with Tata Consultancy Services, Kolkata and Chennai, India. Currently, he is a Transmission Planning Engineer with SaskPower, Saskatchewan, Canada. His research interest includes power system modeling and analysis; in particular, renewable

Ramakrishna Gokaraju (S'88–M'00) received the M.Sc. and Ph.D. degrees in electrical and computer engineering from the University of Calgary, Calgary, AB, Canada, in 1996 and 2000, respectively.

During 1992–1994, he was a Graduate Engineer with Larsen & Toubro-ECC, India; a Research Engineer with Regional Engineering College, Rourkela, India; and a Project Associate with the Indian Institute of Technology, Kanpur, India. During 1999 to 2002, he was a Research Scientist with the Alberta Research Council and a Staff Software Engineer with

IBM Toronto Lab. Currently, he is an Associate Professor with the University of Saskatchewan, Saskatoon, SK, Canada, where he has been since 2003. His current research works are wide-area-based power systems protection and control, renewable energy integrated systems, and real-time simulation approaches.